Chapter 1

Wideband MIMO Measurement Systems for Antenna and Channel Evaluation

Carlos Gómez-Calero, Jonathan Mora, Luis Cuéllar
Leandro de Haro, Ramón Martínez
Technical University of Madrid (UPM)
Spain

1. Introduction

The introduction of new generations of mobile communication systems, such as the current 3G and the future 4G, along with the provision of multimedia services, has exponentially increased the number of users demanding higher data rate. This fact has aroused the interest in studying possible solutions to improve system performance without making use of new frequency band allocations in the already crowded frequency spectrum. As an interesting option, wireless communication systems with Multiple-Inputs and Multiple-Outputs (MIMO) in which many antennas are used for transmission and reception have received increasing attention from the research community over the past few years (Paulraj et al., 2004, Goldsmith et al., 2003).

On the other hand, the OFDM (Orthogonal Frequency Division Multiplexing) technique has been adopted for the transmission of signals over wireless channels in several standards of systems such as DAB, DVB-T and IEEE 802.11a/g for LAN and IEEE 802.16a, for MAN. Moreover, this technique is presented as a potential candidate for the 4G mobile communications. Regarding this, different studies and schemes have been realized to use MIMO systems with OFDM as in (Sampath et al, 2002). In the last two years, the standard IEEE 802.11n is been developing to introduce MIMO with OFDM in WLAN systems.

The performance achieved with a MIMO system depends on factors such as the propagation channel, the space-time processing algorithm, or the number and characteristics of antennas. In order to see MIMO systems deployed over real communication networks, a thorough knowledge of the MIMO channel is a must. Therefore, a significant amount of measurements under real conditions and their detailed analysis are needed. Furthemore, in order to evaluate the performances of MIMO systems regarding the type of antenna array and channel propagation characteristics, two MIMO-OFDM measurement systems have been created in Universidad Politécnica de Madrid (UPM) and described in this chapter.

2. MIMO testbeds

Since MIMO systems begins to be a promising technology for increasing spectral efficiency in the new coming wireless communications systems, many research institutions and universities have been working towards developing some type of MIMO testbeds or prototypes that validated some of the benefits of using multiple antennas at both ends of the radio link.

Development of those platforms is focus on several research topics like MIMO channel for different scenarios, algorithm testing, hardware and software platform employed, coding and modulation techniques, and scope of applications like cellular or wireless LAN.

One of the most dynamic topics has been prototypes showing performance of different MIMO schemes for the mobile Third Generation, 3G. In (Adjoudani et al., 2003), a prototype of 4x4 antennas is integrated in a base station for UMTS system allowing up to 1 Mbps downlink capacity.

Many researchers have been focus in topics regarding wireless LAN standards and applications. Currently, several solutions have been presented as MIMO channel sounders, some of them even at a commercial level. A straightforward implementation is an offline mode operation, which allows implementing the MIMO algorithms and most of the baseband signal processing in a PC-based environment. This operation mode simplifies the algorithms testing, since no real-time constrains have to be fulfilled. In (Batariere et al., 2001) a 2x2 MIMO prototype based in this idea is reported. The signal is pre-calculated, loaded in the transmitter memory and transmitted through the MIMO channel. At the receiver, the raw data is post-processed after being sent to a PC connected to the receiver module. However, this testbed does not include real-time performance evaluation or feedback analysis. Several MIMO testbeds working in offline basis have been presented in (Seeger et al., 2003), (Aschbacher et al., 2004), (Pietsch et al., 2005), (van Zelst et al., 2004).

One of the most world-accepted MIMO channel sounders and with an excellent measurement accuracy and broadband operation is the RUSK channel sounder with MIMO extension, by MEDAV (GmbH, 2001). This channel sounder is based on fast switches to change from one antenna to another. An important drawback of this channel sounder is its very high cost and its low flexibility. Another wideband MIMO testbed is the owned by the Virginia Polytechnic Institute (MCMS testbed) (Ellingson, 2005). It allows up to 4x16 antenna configuration with capabilities like tuning frequency parameter from 250 MHz to 6 GHz with a bandwidth of up to 40 MHz. The signal processing module works over a real 802.11b wireless LAN. A further step in MIMO prototypes systems is carried out by the Georgia Tech (Kaiser et al., Sept. 2004) which is designed for 802.11a and 802.16 standards. It is designed for working in real time basis performing some signal processing tasks over an FPGAs. A similar testbed called "STARS" prototype is presented in (Kaiser et al., 2004) which improves flexibility by configuring multiusers scenarios. Also a few MIMO prototypes with feedback capabilities have been reported. An example of them is presented in (Samuelsson et al., 2005) where a real-implementation of a space-time scheme with wired feedback is presented. Its main advantage is the adaptive modulation and MIMO algorithm testing capabilities. However the system bandwidth is very small.

Some commercial prototypes can be considered as general purpose platforms for MIMO testing, measuring and developing of algorithms. An interesting example is the HaLo prototyping platform, from (Signalion). It consist of a flexible and scalable hardware platform that includes some of the basic modules to be used in a real-time implementation and easy-to-use interface with MATLAB/Simulink flow, and several reference modules for the simulation of the physical layer of 802.11a/n standards, among others. An implementation of a 4x4 MIMO-OFDM testbed using the HaLo prototype was presented in (Stege et al., 2004). For more extensive resume of MIMO testbeds the reader can review the first part of (Kaiser et al., 2004).

3. Measurement system for 2.45 GHz MIMO channels

In this section, a description of design and implementation of a measurement system (testbed) at 2.45 GHz is detailed. The testbed UMATRIX (UPM Multi-Antenna Testbed for Research in Indoor eXperiments) is based on Software-Radio and it works at 2.45 GHz. One of the most important advantages of this testbed is that it can realize measurements in MIMO-OFDM channels with different types of antenna and configurations, such as reconfigurable antennas.

The general scheme of MIMO testbed UMATRIX is shown in Fig. 1. It allows the use up to 4 antennas at the transmitter and the receiver side, so a 4x4 MIMO scheme can be evaluated. The way of working is the following: in the first place, the OFDM signals for all the antennas are generated in an offline mode in the PC by Matlab. Once the signals are generated, they are introduced to online processing module, which consists of SDR (Software-Defined Radio) platforms and it sends the signals to RF subsystem. This is the IF/RF module and its objective is to amplifier, filter and upconvert the signals to RF (2.45 GHz). The last module in the transmitter is the antenna one, which receives the signals from RF stage and send them to the receiver through MIMO channel.

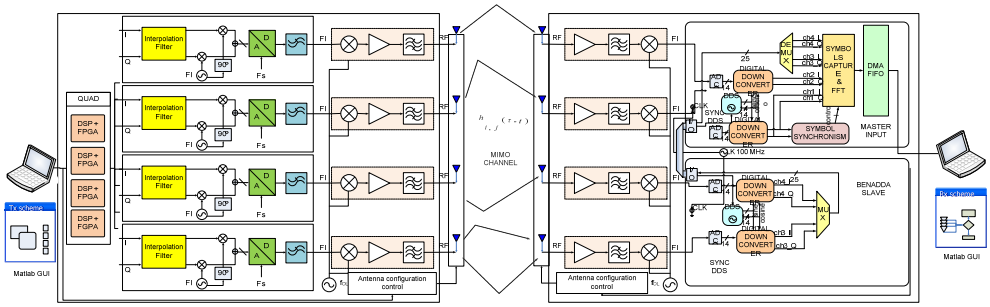

Fig. 1. General scheme of UMATRIX

At the receiver side, the signals are received by the antennas and passed to RF/IF stage which downconverts the signals to IF (40.625 MHz). From here, the signals go to SDR which are based on a FPGA design with 2 boards: one for receivers 1 and 2, and another for 3 and 4. This module process the OFDM signals in time and send them in frequency domain to the

PC in order to do a pos-process (offline) to obtain the channel response. Moreover, a new module has been added to control the different configurations of reconfigurable antenna under test.

3.1 Signal processing

The signal processing subsystem deals with all the different modules which are related to the OFDM signal, the software-radio and the channel estimation.

3.1.1 OFDM structure

Due to have a demonstrator of wideband, the OFDM technique will be used, since is very efficient to transmit data over selective frequency fading channels. The main idea is to divide in frequency a wideband channel in narrowband subchannels. Likewise, each subchannel is a channel with flat fading despite of frequency-selective feature of a wideband radio channel. To generate these subchannels in OFDM, an inverse of Fourier Fast Transformation (IFF) is applied to one block of *N* data symbols:

$$x(n) = \frac{1}{N}\sum_{k=0}^{N-1} X(K) e^{j\frac{2\pi f_c kn}{N}} \tag{1}$$

In order to avoid inter-symbol interference due to the spreading of channel delay, a cyclic-prefix block is inserted. This prefix is known as guard interval (GI), where the number of samples of th prefix should be higher than the length of channel impulse response. The effects of cyclic-prfix delete the ISI and convert the convolution between transmitted symbols and channel in a circular convolution. Thus, the FFT is used at the receiver to recover the block of data symbols. The synchronism module in the FPGA of the receiver is based on (van de Beek et al., 1997). In Table 1 the most important parameters of the system are detailed.

Parameter	Symbol	Value
Sampling frequency	Fs	6.25 MHz
Useful symbol time	Tu	1024/Fs=163.84 μs
Guard time	Tg	Ts/8=40.96 μs
Symbol time	Ts	184.32 μs
Spacing between carriers	Δf	1/Tu≈6.1 KHz
Number of carriers	N	768
Bandwith	BW	4687500 Hz

Table 1. Main testbed OFDM parameters

In the transmitter, a frame with 8 OFDM symbols is continuously generated, as shown in Fig. 2. The first symbol is used for receiver synchronism and is a null symbol. After that, a reference symbol which will be used to estimate the channel is introduced. And finally, 6 data symbols are included. These symbols are randomly generated since they are not going to be evaluated, only the reference symbol to obtain the channel response.

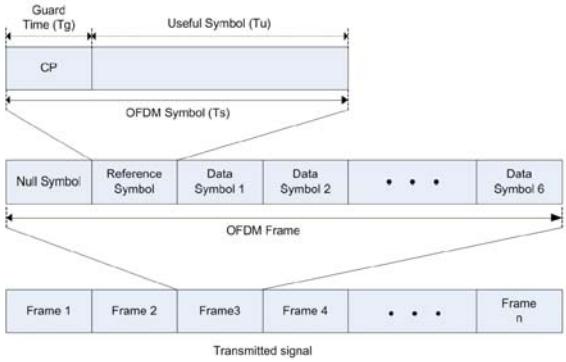

Fig. 2. OFDM frame structure

3.1.2 Channel estimation

The channel estimation in MIMO systems is a very important stage, since in MIMO systems the performances of algorithms depend on the accuracy of this estimation. The received signal in each carrier is given by

$$\mathbf{R}_k = \mathbf{H}_k \mathbf{X}_k + \mathbf{N}_k \tag{2}$$

where **X** is the vector of transmitted signals by each antenna, **H** indicates the MIMO channel matrix and **N** represents the noise in the channel, all for each *k*-th subcarrier. The MIMO channel matrix can be computed by

$$\mathbf{H}_k = \begin{bmatrix} h_{1,1,k} & \cdots & h_{1,M_T,k} \\ \vdots & \ddots & \vdots \\ h_{M_R,1,k} & \cdots & h_{M_R,M_T,k} \end{bmatrix} \tag{3}$$

where each element of the matrix represents the channel response between each pair of transmitter and receiver antennas.

On the other hand, different ways of obtaining the channel response have been studied. In UMATRIX, orthogonal codes are used as pilots to let the receiver split the different contributions from each antenna. Due to the maximum number of antennas is 4, a 4x4 matrix is needed. In our case, we use the following pilot matrix:

$$\mathbf{P} = \begin{bmatrix} 1 & -1 & 1 & 1 \\ 1 & 1 & -1 & 1 \\ 1 & 1 & 1 & -1 \\ -1 & 1 & 1 & 1 \end{bmatrix} \tag{4}$$

where the number of rows represents the space and the columns can represent either the time or the frequency. In a firs option, the frequency axis was chosen, so in this way, the

channel is assumed invariant in 4 subcarriers. However, and with the aim of measuring frequency selective channels, the time was as chosen axis in columns.

In order to get a better synchronization at the receiver, the pilot matrix **P** is multiplied by a pseudorandom sygnal (S). Thus, at the receiver, for each *k*-subcarrier, we will have (2) with

$$\mathbf{X}_k = S_k \mathbf{P} \tag{5}$$

And if it is chosen

$$\mathbf{Y}_k = \mathbf{X}_k^H \left(\mathbf{X}_k \mathbf{X}_k^H \right)^{-1} \tag{6}$$

to estimate the channel, then the channel is multiplied by received signal **Y**, obtaining:

$$\begin{aligned} \hat{\mathbf{H}}_k &= \mathbf{R}_k \mathbf{Y}_k \\ &= \mathbf{H}_k \left(S_k \mathbf{P} \right) \mathbf{Y}_k + \mathbf{N}_k \mathbf{Y}_k \\ &= \mathbf{H}_k + \mathbf{N}_k \mathbf{Y}_k \end{aligned} \tag{7}$$

In Fig. 3. the estimated MIMO channel is plotted using the previous scheme of testbed. To do it, each transmitter antenna was connected to each correspondent receiver antenna (h_{11}=h_{22}=h_{33}=h_{44}=*1*), with the aim of testing the orthogonality of pilots.

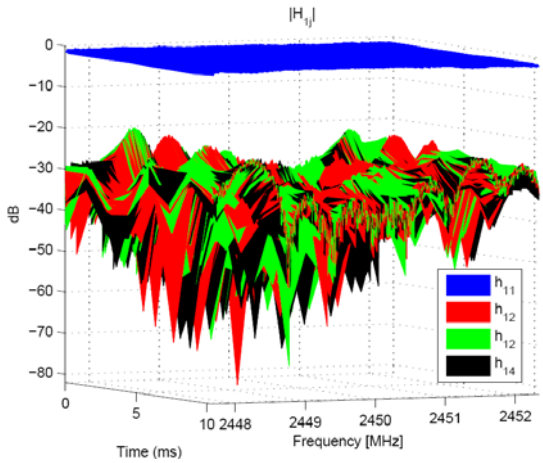

Fig. 3. Orthogonality of the pilot code to estimate the channel

3.2 Antennas

For each combination of transmitter and receiver locations, three types of antennas have been used: firstly the monopole array were utilized at both the receiver and the transmitter, in order to evaluate the system performance when only vertical polarization is used. Afterwards, the dual-polarized antennas (crossed dipoles) were used, so polarization diversity is included in the system, to the cost of reducing spatial diversity (since the dual-

polarized dipoles are co-located). And finally, a planar inverted-F antenna (PIFA) array with 2 elements was placed to be evaluated (Gómez et al, 2008).

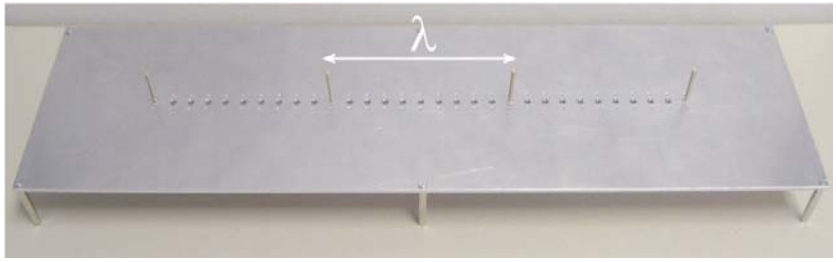

a) Monopoles

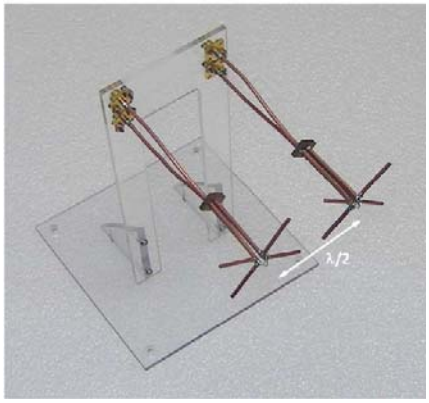

b) Cross-polarized dipoles

c) PIFAs

Fig. 4. Antennas under test

3.3 Measurements

3.3.1 UMATRIX application

One of the main objectives of the UMATRIX is that it has to allow measurements of reconfigurable antennas in different environments. Thus, a tool with a friendly-user interface and easy to use has been development in Matlab for the integration of processing and measurement parts. In Fig. 5. the main window of the application is shown, where the user goes checking the measured points, received signals and MIMO channel capacity obtained.

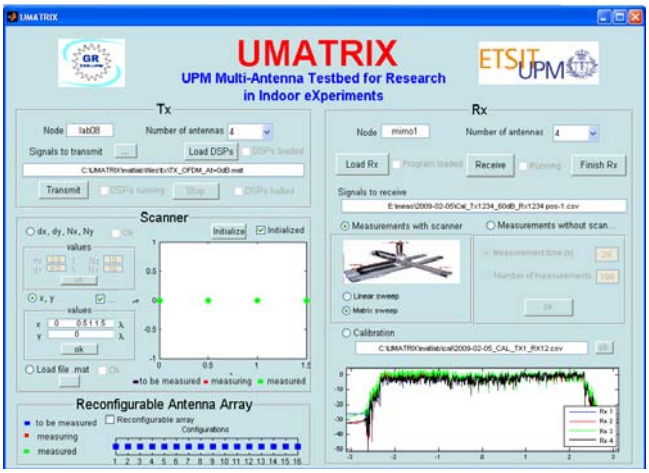

Fig. 5. Main window of UMATRIX

Fig. 6.a) shows the transmitter of UMATRIX where the antenna array is located at the top. All the transmitter is placed in a mobile platform to put it in several locations. On the other hand, the receiver has a scanner which can sweep any point within an area of 6λx6λ (Mora et al., 2008). Fig. 6.b) depicts the receiver with the scanner and the antenna array in the scanner.

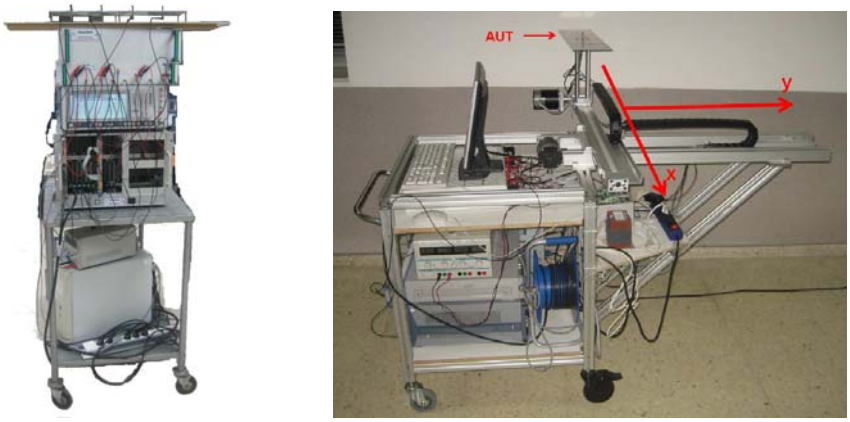

a)Transmitter b)Receiver

Fig. 6. Implementation of the testbed

3.3.2 Locations

All the measurements were taken in the ETSI de Telecomunicación (Madrid), in the fourth floor of building C. In Fig. 7. different types of measurements can be distinguished regarding the scenario: office and corridor. For the corridor environment, the transmitter was put at the end of the corridor and the receiver was located in position 1 for LoS and

positions 2 and 3 for NLoS situations. In the case of office scenario, the transmitter was placed in a laboratory (Tx B in Fig. 7.) and the receiver in another office.

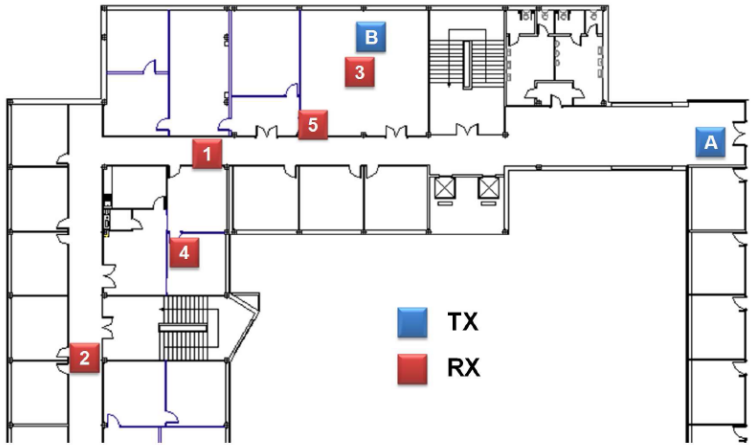

Fig. 7. Map of locations in the measurements campaigns

3.3.2 Results

Once the channel is obtained in the receiver, the MIMO channel capacity is calculted. Previously, the **H** matrix is normalized with the Frobenius norm. In order to remove the path loss effect and study the diversity characteristics of the MIMO propagation channel, the channel matrix **H** is usually normalized to obtain a fixed local signal to noise ratio for each measured point. The use of this normalization is equivalent to considering a perfect power control in the system. This is interesting to characterize the multipath richness and diversity offered by the propagation environment, but it does not take into account the path loss, shadow fading and penetration losses. Then the normalized channel will be

$$\mathbf{H}_{norm} = \sqrt{M_T \cdot M_R}\,\frac{\mathbf{H}}{\|\mathbf{H}\|_F} = \sqrt{M_T \cdot M_R}\,\frac{\mathbf{H}}{\sqrt{\sum_{i=1}^{M_T}\sum_{j=1}^{M_R} h^{ref}{}_{ij} \cdot h_{ij}^{ref*}}} \tag{8}$$

where $\mathbf{I}_{MR}$ is the identity matrix of size M_RxM_R, M_T is the number of transmitter antennas. To compare the capacities for different types of antenna, a normalization with one antenna array in each type of scenario has been done. On the other hand, as the channel state information is not known at the transmitter, the capacity (in bps/Hz) in each k subcararier is calculated from

$$C_k = \max_{\mathbf{Q}} \log_2 \left[\det\left(\mathbf{I}_{M_R} + \frac{\rho}{M_T} \mathbf{H}_k \mathbf{Q} \mathbf{H}_k{}^H \right) \right] \tag{9}$$

where **Q** is the covariance matrix of transmitted signals, such that Tr{**Q**} ≤ M_T to account for power constraint, ρ is the signal to noise ratio at the receiver, $(\cdot)^H$ denotes Hermitian and $|\mathbf{A}|$ is the determinant of matrix **A**. Two cases were considered in this analysis: no channel state information (CSI) at transmitter and total CSI at transmitter. In the first case, the power

allocation strategy is assumed to be uniform, so that the channel capacity expression may be simplified to

$$C_k = \log_2\left[\det\left(\mathbf{I}_{M_R} + \frac{\rho}{M_T}\mathbf{H}_k\mathbf{H}_k^{\,H}\right)\right] \tag{10}$$

When total CSI at transmitter is considered, the optimum waterfilling scheme is assumed to allocate power, so the singular value decomposition (SVD) of **H** is realized, and the capacity is computed as

$$C_{WF} = \sum_{i=1}^{K} \ln\left(\mu\lambda_i\right)^+ \tag{11}$$

where $(\cdot)^+$ denotes taking only those terms which are positive, and λ_i is the i (out of k) non-zero eigenvalue of the correlation channel matrix $\mathbf{R}=\mathbf{H}\mathbf{H}^H$. The parameter μ is chosen to satisfy the power constraint

$$\rho = \sum_{i=1}^{K}\left(\mu - \frac{1}{\lambda_i}\right)^+ \tag{12}$$

For 4x4 MIMO channel measurements, a comparison of single with dual-polarization performances was realized for each scenario. Fig. 8. shows the capacity obtained for the corridor scenario with LoS (position 1 of the receiver in Fig. 7.). As it is shown in Fig. 8.a), the capacity increases with the spacing between elements, except for the case of 0.3λ. The knowledge in the transmitter can give an extra capacity, as Fig. 8.b) depicts. The use of Waterfilling scheme improve the performances in all the SNR range.

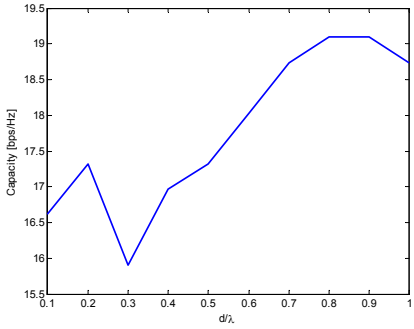

a) Capacity of monoples array as a function of spacing with a SNR=20dB

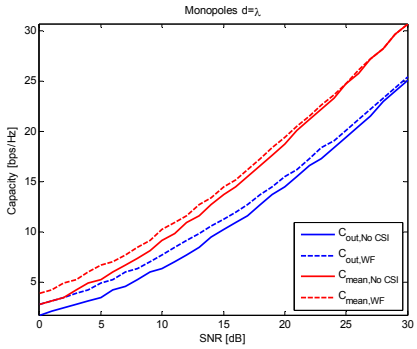

b) Comparison of monopoles capacity with a spacing of λ, as a function of SNR and CSI

Fig. 8. Capacity of monopole array.

On the other hand, the importance of using single or dual polarization has been also studied. Fig. 9. represents the CDF of the capacity for all the monopole array spacings and the cross-polarized dipole array. It is shown that for LoS the employ of dual polarization enhances the performances with respect to the MIMO channel capacity. However, for NLoS cases, the use of dual polarization does not have a great impact on the performances.

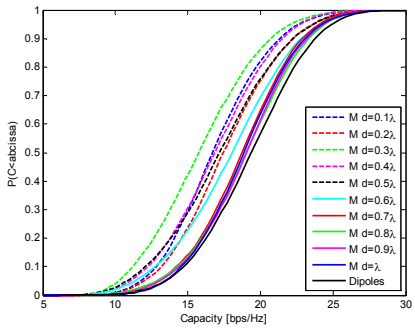

a) CDF capacity of corridor LoS (position 1 of Fig. 7.)

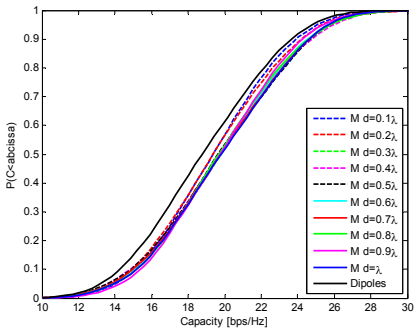

b) CDF capacity in NLoS scenario (position 3 of Fig. 7.)

Fig. 9. Comparison of the CDF capacity for single and dual polarization antennas.

Moreover, 4x2 MIMO channel measurements were carried out to compare the MIMO channel capacity by using different radiating elements. Fig.10. compares the CDF of the capacity obtained for monopoles, dipoles and PIFAs in different scenarios, with LoS and NLoS. It can be concluded that for two radiating elements at the receiver side, MIMO channel capacity strongly depends on the antenna characteristics, such as radiation pattern, mutual coupling and spacing between elements.

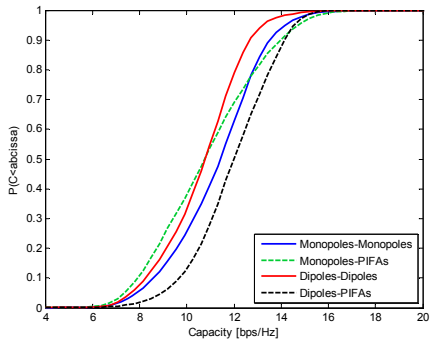

a) CDF capacity of corridor LoS (position 1 of Fig. 7.)

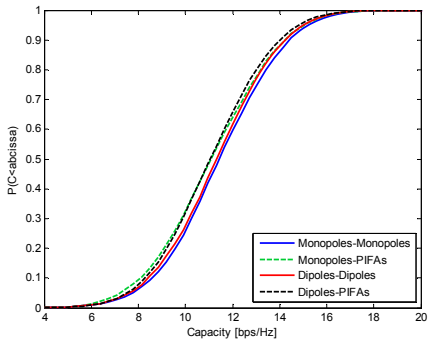

b) CDF capacity in NLoS scenario(position 4 of Fig. 7.)

Fig. 10. Comparison of the CDF capacity for 4x2 MIMO channels with different antennas

4. MIMO prototype for DVB-T2 system

DVB-T2, the second generation of the DVB proposal for digital terrestrial TV, has been recently proposed by DVB project (dvb) as an evolution of DVB-T when the shutdown of analog television process will be finished. In order to give a newer technical response to the necessity the digital dividend, process by which some free frequencies at UHF used by analog TV will be assigned to different services (3G/4G), DVB-T2 will improve frequency efficiency to provide multicast in HD with the same 8 MHz channel.

As DVB-T, DVB-T2 expects to be received in plugged TV terminals in mobile environment or with unplugged terminals in indoor or in low speed (pedestrian) environments, so a MISO scheme has been included, transmitting with a distributed Alamouti block code. However, in order to go further a full MIMO scheme is proposed in this paper, which may be similar to the one that will be included in NGH (second generation of DVB-H) in the next future, obtaining a very efficient performance in highly Doppler environments, that is to terminals (unplugged or not) operating in high speed vehicles.

On the other hand, DVB-T2 will provide higher efficiencies in frequency than the nowadays DVB standard DVB-T. DVB-T2 proposal considers the inclusion of MISO technology but not MIMO. MIMO will be considered in future revisions and it will provide a further increment of frequency efficiency mainly in harsh scenarios as strong multipath environments or highly Doppler radio channels.

In order to evaluate the performances of a DVB-T2 system in realistic scenarios, the use of a real platform is of great interest, since it enables to include several aspects that are not usually addressed in theoretical studies or simulations, such as the effect of different antennas or scenarios (Gómez-Calero et al., 2006). In this section, a novel 2x2 MIMO testbed for DVB-T2 has been designed and implemented in order to test the enhancement obtaining by the using of multiple antennas at each side of the radio link for UHF band, particularly at frequency of 594 MHz.

The general architecture of the testbed is depicted in Fig. 11., where 2 antennas can be placed at the transmitter and the receiver side. The DVB-T2 signals are generated off-line in a PC (e.g. using Matlab) and then they are sent to the Software-Defined-Radio (SDR) platform. This platform receives the signals and transmits them in real-time and in Intermediate Frequency (IF) to the RF module. Finally, signals are upconverted to RF frequency, amplified and filtered, and then transmitted to the radio channel by the antenna array. In the receiver, the signals are captured by the antenna array and downconverted, amplified and filtered by the RF module. Finally, the SDR realizes the synchronization and FFT previous to send the signals to the PC.

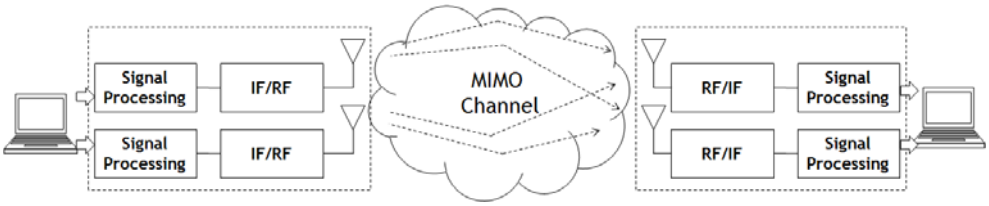

Fig. 11. General architecture of the MIMO measurement system for DVB-T2

4.1 Signal processing

The most complex part of the testbed is the signal processing module, since it supports all the digital to analog and analog to digital conversions (DAC and ADC) and the processing of the OFDM signal with the synchronization and the use of the Fast Fourier Transmorm

(FFT). In the following subsections the transmitted DVB-T2 signals and SDR platform are explained.

4.1.2 DVB-T2 structure

The DVB-T2 frame structure is divided in three different parts (ETSI, 2008). The first one is the P1 symbol which is used to do a faster detection and frequency synchronization. Then, the P2 symbol is transmitted to indicate the type of encoders and data configuration of the data symbols. However, for the sake of simplicity in this testbed the P2 symbol is removed. Finally the data symbols are sent with the user data and pilots for the channel estimation.

The block diagram of the transmitter is shown in Fig. 12. Data are generated and passed to the MIMO encoder which applies the distributed Alamouti to transmitt the signals by each antenna and then to recover the data symbols in the receiver. The Alamouti scheme (Alamouti, 1998) is modified with the scheme detailed in Table 2.

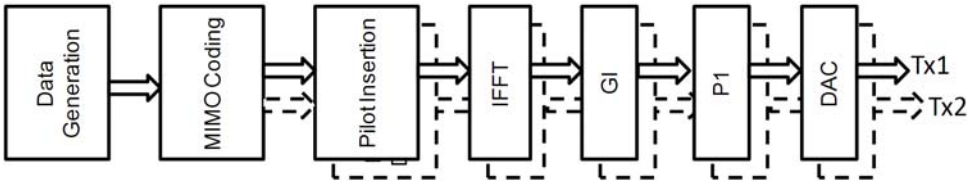

Fig. 12. Block diagram of the transmitter signal processing

Subcarrier	Tx antenna 1	Tx antenna 2
k_i	s_1	$-s_2^*$
k_{i+1}	s_2	s_1^*

Table 2. Alamouti modified scheme

After that, the continual and scattered pilots are inserted to estimate the channel at the receiver. Then, the Inverse-FFT (IFFT) is done and the Guard Interval (GI) is inserted in order to avoid inter-symbol interference (ISI) due to the channel delay spread. The cyclic-prefix removes the ISI and converts the convolution between transmitted symbols and channel into a circular convolution. Finally, the P1 symbol is inserted and the two signals are converted from digital to analog and sent to RF module.

4.1.3 Sowtfare-Radio

For the real-time process, two XtremeDSP boards based on the BenADDA module of Nallatech have been used: one for the transmitter and one for the receiver. Each board has a FPGA VirteX II Pro V2P30 and 4 MBytes of SRAM memory with 2 DACs of 160 MHz and 2 ADCs of 105 MHz (Nallatech).

Fig. 13. shows the architecture of the transmitter. The data symbols are sent to the board via DMA through the PCI bus. The DMA SRAM IFACE module stores them in the board external memory ZBT SRAM. The maximum capacity is 512 samples per channel. Once the data write cycle is finished, the same module reads them from the memory and extracts

them in a continuous and cyclic way. The I/Q data streams of each channel go to *Digital Up Converter* module, where the signals are interpolated by a factor of 10 and are upconverted to an IF of 36 MHz. The data are sent to DACs, which operate at a frequency of 91428571 Hz. This frequency is selected for being 10 times the inverse of the sample period of a 8 MHz channel, which according to the DVB-T2 standard (ETSI, 2008) is T=7/64 μs.

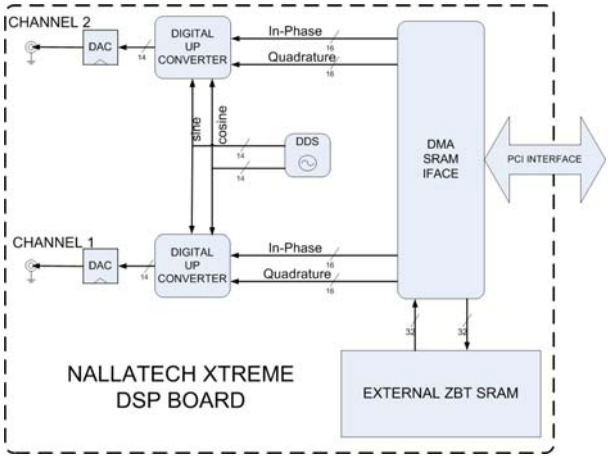

Fig. 13. Architecture of SDR transmitter

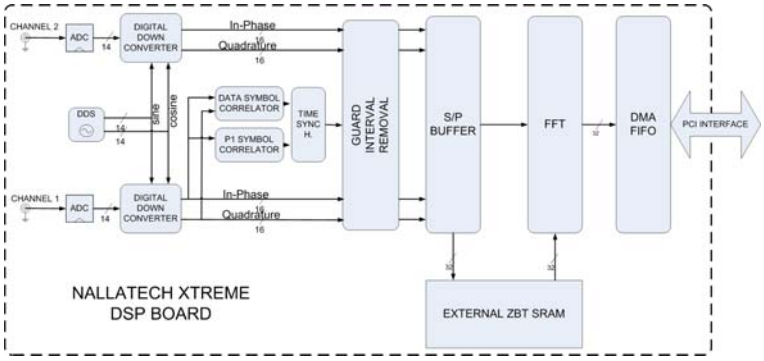

Fig. 14. Architecture of SDR receiver

On the other hand, Fig. 14. represents the main blocks of receiver subsystem. The signal from channel 1 is used to obtain the synchronism in time domain of received symbols. The synchronism algorithm is based on the correlation of the cyclic prefix of OFDM symbols (van de Beek et al., 1997). Then, the signals go to *Time Synch* module which generates the synchronism signal which allows to obtain the OFDM symbols in the next module, named *Guard Interval Removal*. Finally, the FFT is done to recover the block of data symbols.

In order to estimate the beginning of the frame, the signal passes through a correlator with the P1 symbol. Fig. 15. represents the correlation of a frame made up a P1 symbol and 9 data symbols.

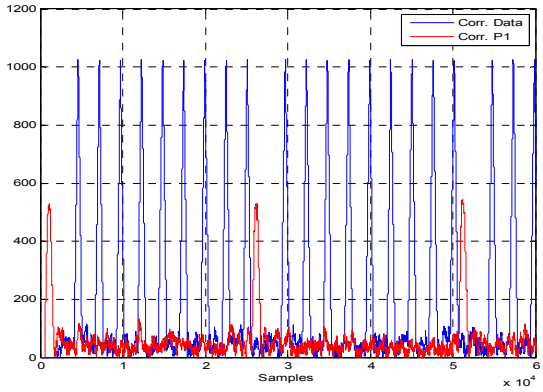

Fig. 15. Correlation of received signals. Red line represents the correlation with the P1 symbol and blue line shows the autocorrelation with the data symbol

4.1.5 Channel estimation

One of the key aspects in MIMO is the channel estimation, since MIMO system performances depend on the accuracy of the estimated channel matrix. Due to the selection of 2K mode of FFT and a GI of 1/8, the DVB-T2 standard (ETSI, 2008) proposes the PP1 pattern for scattering pilots for MISO.

The scattered pilots, for each OFDM symbol are placed each 12 subcarriers along the frequency axis. Attending to the temporal axis, the pilots start in the first subcarrier and the initial point is shifted in 2 subcarriers for the following 3 OFDM symbols, as Fig. 16.a) and Fig. 16.b) show for antenna 1 and 2, respectively. Thus, the pilots structure is done in 4-symbol blocks in time domain and it depends on the used antenna. In antenna 2 case (Fig. 16.b), the corresponding pilots to symbols 1 and 3 are inverted to distinguish the transmitter antenna. Moreover, it is worth mention here that the scattering pilots are generated according to a pseudorandom sequence and PRBS (ETSI, 2008).

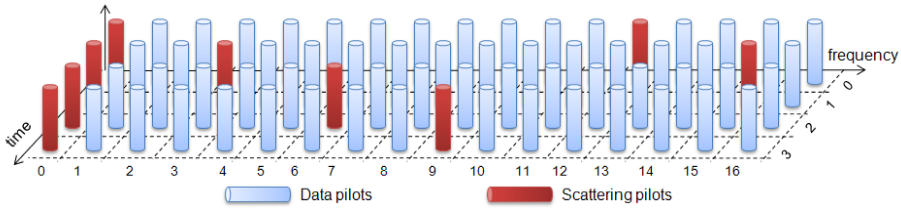

a) Antenna 1

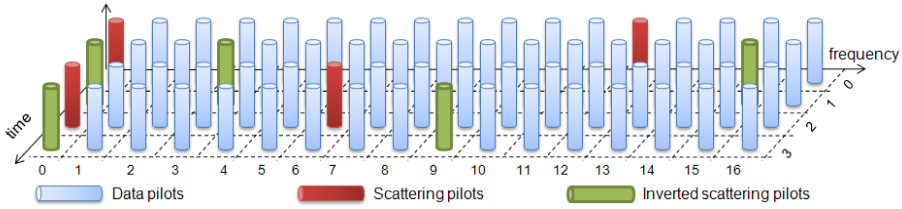

b) Antenna 2

Fig. 16. Scattered pilots distribution

Thus, if $\mathbf{X}_k$ represents the transmitted symbols vector for both antennas for the k-subcarrier, the received vector $\mathbf{R}_k$ is given by (2). Due to the testbed has two antennas in the transmitter and other two in the receiver, the MIMO channel matrix is represented by

$$\mathbf{H}_k = \begin{bmatrix} h_{1,1,k} & h_{1,2,k} \\ h_{2,1,k} & h_{2,2,k} \end{bmatrix} \tag{13}$$

where each matrix element indicates the subchannel between each pair of transmitter-receiver antenna.

In the literature a MIMO channel estimator for DVB-T2 has not been proposed, so in this section an original scheme is presented to estimate the channel for MIMO case. First of all, the channel is asummed not to vary in time domain for 4 data symbols, similar to other channel estimators for DVB-T (Lee et al., 2007, Palin & Rinne 1999, Chen et al., 2003, Fang & Ma, 2007). Therefore, the pilots are gathered in groups of 4 OFDM data symbols in only one symbol, obtaining one pilot subcarrier out of 3 subcarriers. Fig. 17. depicts the association for both antennas.

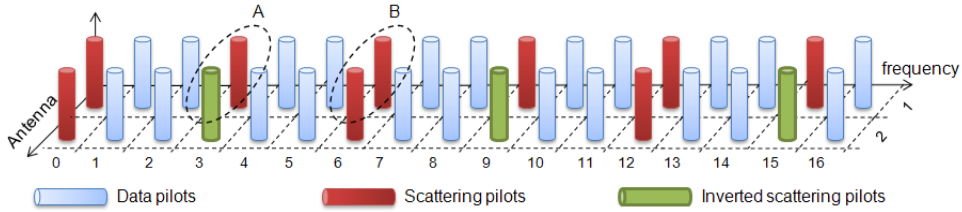

Fig. 17. Scattered pilots association for antennas 1 and 2

The received signals in antennas 1 and 2, $r_{1,k}$ and $r_{2,k}$, respectively, for the k-subcarrier are given by

$$\begin{aligned} r_{1,k} &= x_{1,k} \cdot h_{11,k} + x_{2,k} \cdot h_{12,k} + n_{1,k} \\ r_{2,k} &= x_{1,k} \cdot h_{21,k} + x_{2,k} \cdot h_{22,k} + n_{2,k} \end{aligned} \tag{14}$$

where $x_{i,k}$ represents the pilot signal transmitted by antenna i, and $n_{i,k}$ is the noise contribution in antenna i. From this point Here, two cases are considered to estimate the

channel. The first one is the case in which the pilots of both antennas are scattered pilots for a given subcarrier. This case is marked with ***A*** in Fig. 17. In the other case, the pilot for one antenna is a scattered pilot and for the other antenna is an inverted scattered pilot, for a given subcarrier. This is case ***B*** in Fig. 17.

Thus, for case A the received signals are

$$\begin{aligned} r^a_{1,k} &= x^a_{1,k} \cdot h_{11,k} - x^a_{1,k} \cdot h_{12,k} + n^a_{1,k} \\ &= x^a_{1,k} \cdot (h_{11,k} - h_{12,k}) + n^a_{1,k} \end{aligned} \tag{15}$$

$$\begin{aligned} r^a_{2,k} &= x^a_{1,k} \cdot h_{21,k} - x^a_{1,k} \cdot h_{22,k} + n^a_{2,k} \\ &= x^a_{1,k} \cdot (h_{21,k} - h_{22,k}) + n^a_{2,k} \end{aligned} \tag{16}$$

And for case B

$$\begin{aligned} r^b_{1,k} &= x^b_{1,k} \cdot h_{11,k} + x^b_{1,k} \cdot h_{12,k} + n^b_{1,k} \\ &= x^b_{1,k} \cdot (h_{11,k} + h_{12,k}) + n^b_{1,k} \end{aligned} \tag{17}$$

$$\begin{aligned} r^b_{2,k} &= x^b_{1,k} \cdot h_{21,k} + x^b_{1,k} \cdot h_{22,k} + n^b_{2,k} \\ &= x^b_{1,k} \cdot (h_{21,k} + h_{22,k}) + n^b_{2,k} \end{aligned} \tag{18}$$

Operating with the obtained signals from (15)-(18), channel coefficients can be estimated as

$$\tilde{h}_{1,1,k} = \frac{r^a_{1,k} + r^b_{1,k}\left(\frac{x^a_{1,k}}{x^b_{1,k}}\right)}{2x^a_{1,k}} \tag{19}$$

$$\tilde{h}_{1,2,k} = \frac{r^a_{1,k} - r^b_{1,k}\left(\frac{x^a_{1,k}}{x^b_{1,k}}\right)}{-2x^a_{1,k}} \tag{20}$$

$$\tilde{h}_{2,1,k} = \frac{r^a_{2,k} + r^b_{2,k}\left(\frac{x^a_{1,k}}{x^b_{1,k}}\right)}{2x^a_{1,k}} \tag{21}$$

$$\tilde{h}_{2,2,k} = \frac{r^a_{2,k} - r^b_{2,k}\left(\frac{x^a_{1,k}}{x^b_{1,k}}\right)}{-2x^a_{1,k}} \tag{22}$$

And the estimated MIMO channel matrix is

$$\tilde{\mathbf{H}}_k = \begin{bmatrix} \tilde{h}_{1,1,k} & \tilde{h}_{1,2,k} \\ \tilde{h}_{2,1,k} & \tilde{h}_{2,2,k} \end{bmatrix} \tag{23}$$

4.2 RF-FI

In the transmitter, the RF stage receives the signal from signal proccesing module and upconverts from IF (36 MHz) to RF frequency (594 MHz). Then, the signal is filtered and amplified, with a transmitted power of +2 W rms. In order to upconvert the signals of both branches 1 and 2, a direct digital synthesizer (DDS) is used.

In the receiver, the signals are received from antenna ports and then are amplified, filtered and downconverted to IF. In this case, a voltage controlled attenuator is placed to adapt the recevied signal power to the best range of levels. The variation of the attenuator is from 3 dB to 38 dB in steps of 5 dB.

4.3 Antenna array

The MIMO testbed has two antennas at the transmitter and two at the receiver, respectively. The antennas have been designed for the testbed to work at 594 MHz. The radiating element is a dipole with a reflector element**.** The reflection coefficient of the transmitter and receiver antennas is depicted in Fig. 18.a). It shows that all the implemented antennas have a good matching at desired frequency band, obtaining a reflection coefficient lower than -17 dB. On the other hand, the radiation pattern is presented in Fig. 18.b), where the XPD is higher than 25 dB in the maximum direction of $\theta=0^{o}$.

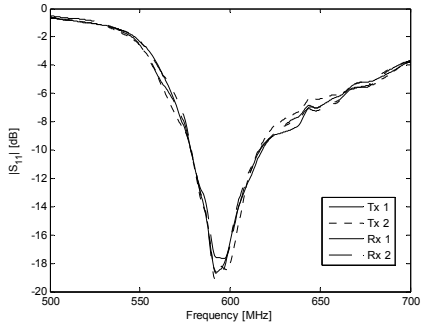

a) Reflection coefficient of the antennas

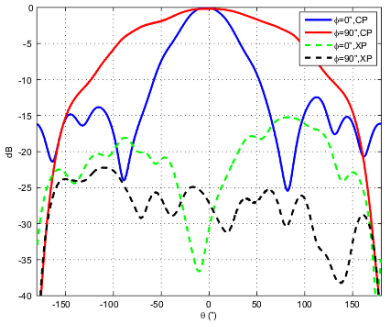

b) Measured radiation pattern of an antenna

Fig. 18. Antenna performances

4.5 Measurements in indoor/outdoor scenarios for different polarizations

Once the different modules of transmitter and receiver are implemented and work properly, the integration of all of them is done. In Fig. 19. the transmitter and receiver are illustrated. The transmitter is placed on a 19" rack and the received is mounted on a mobile platform in order to measure different environments.

a) Transmitter

b) Receiver

Fig. 19. Integration of the testbed

As in any real system, implementation issues such as frequency errors by using different local oscillators internal clocks at each side of the radio link appear. In general, all the errors can be represented as

$$\mathbf{R}_k = \mathbf{H}_k \mathbf{X}_k \cdot \left(\exp\left(j\left[2\pi k \frac{Td}{Tu} + 2\pi k \frac{\Delta t}{Tu} + \phi_0 + 2\pi k \Delta f Ts \right] \right) \right) + \mathbf{I}_k + \mathbf{N}_k \qquad (24)$$

where T_d represents the symbol temporal offset, Δ_t the sampling temporal offset, φ_0 the phase offset, Δ_f the frequency offset and $\mathbf{I}_k$ is the ICI (Inter-Carrier Interference) due to frequency offset for the *k*-carrier. These errors must be taken into account and have been mitigated in the signal processing module.

Once the MIMO testbed has been realized, a measurement campaign has been carried out in order to evaluate the enhancement obtained by using the MIMO scheme. The measurements were carried out in the E.T.S.I of Telecommunications School, at Universidad Politécnica de Madrid, Spain. The transmitter was situated on the rooftop of building C with a spacing between elements of λ. Fig. 20. depicts the topview of the measurement locations. In order to measure several scenarios, the receiver was located in three different positions. In position 1, the receiver was placed in the parking area of the building in LoS (Line of Sight). The receiver for NLoS (Non Line of Sight) was situated in position 2, in the parking of the next building. Finally, for the indoor scenario, the receiver was located in the third floor of the building, as Fig. 20. shows. For each scenario, three different polarization schemes were evaluated: HH, HV and VV, where H and V means horizontal and vertical polarization for antennas 1 and 2 both in the transmitter and the receiver, respectively.

Fig. 20. Top view of the Tx and Rx positions

4.5.1 MIMO channel

The first step for evaluating the MIMO channel is to normalize channel power. After chanel estimation, the channel power is calculated for all the measured cases. The channel power is averaged over all frequencies f_v and temporal snapshots t_u and is calculated by

$$P_{avr} = \frac{\sum_{i=1}^{N_t}\sum_{j=1}^{N_f} P(t_u, f_v)}{M_T M_R} \tag{25}$$

where N_t represents the number of OFDM symbols (100 in this case), N_f indicates the number of subcarriers (2048) and P represents the mean power in the measured point and is given by

$$P(t_u, f_v) = \frac{\| P(t_u, f_v) \|_F^2}{M_T M_R} \tag{26}$$

Table 3 shows the comparison of mean power for each scenarios as a function of antenna polarization. It is shown in LoS scenarios, the received power is increased. However, in indoor case the power only is reduced in 6 dB because the distance between the transmitter and receiver is about 23 m smaller than in the case 3.

Measured scenario	Mean channel power (dB)		
	HH	HV	VV
1 - Outdoor LoS	-63.5	-62.8	-63.2
2 - Outdoor NLoS	-81.1	-81.8	-73.7
3 - Indoor NLoS	-67.9	-68.8	-69.5

Table 3. Comparison of measured mean power

4.5.2 MIMO capacity

Besides the diversity gain, the other important of MIMO channels is the increase of the channel capacity. In the case of DVB-T2, the transmitter does not know the Channel State Information (CSI), and the MIMO capacity can be calculated from

$$C_k = \sum_{k=1}^{N} \log_2 \left[\det \left(\mathbf{I}_{M_R} + \frac{\rho}{M_T} \mathbf{H}_k \mathbf{H}_k^{H} \right) \right] \text{ bps/Hz} \tag{27}$$

where M_R and M_T represent the number of receiver and transmitter antennas, respectively, k is the given subcarrier, N represents the total number of subcarriers and ρ is the Signal to Noise Ratio (SNR). The measurements have been realized with M_T=M_R=2.

With the aim of comparing the capacity of SISO and MIMO, Fig. 21. represents the cummulative distribution function of the capacity calculated for the LoS case with polarization diversity. The capacity increases in the 2x2 case.

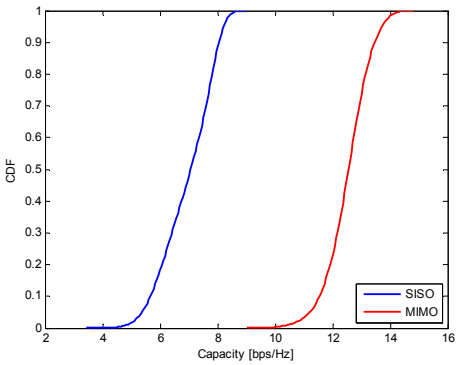

Fig. 21. Comparison of CDF of capacity with 1x1 and 2x2 in outdoor LoS case with polarization diversity

On the other hand, Fig. 22. shows the comparison of all the cases comparing the use of different polarization schemes. The highest values of capacity are obtained for indoor NLoS, followed by outdoor NLoS and the, outdoor LoS, except when polarization diversity (HV) is used in LoS case, since the obtained outage capacity at 10% is the highest.

Attending to outage capacity, the highest values are obtained for the outdoor LoS HV case and the indoor situations for all the polarization schemes.

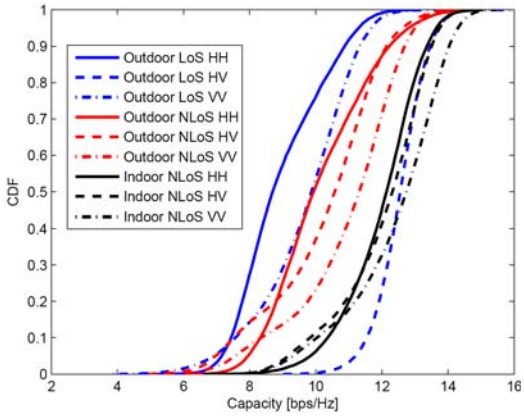

Fig. 22. CDF of capacity for all the measured scenarios

5. Conclusions

In the last decade, Multiple-Input Multiple-Output (MIMO) systems have created a great interest in research. Many works shows an increase in terms of data bit rate by using several antennas at each side of the radio link. In this chapter, two novel measurement systems for MIMO channels in indoor environment are presented. In order to study the propagation characteristics of these systems, using both polarization and spatial diversity in multi-antenna systems can be evaluated, thanks to the use of different types of antennas.

On one hand, a novel MIMO-OFDM testbed (UMATRIX), designed and implemented in the UPM, has been used to accomplish the measurements at 2.45 GHz. The UMATRIX has several characteristics which makes it good for antenna reconfigurable measurements. OFDM technique is introduced to measure the wideband MIMO channel response, so a FPGA-based receiver has been developed. A measurement campaign to compare the system performance with either single-polarized or dual-polarized antennas was conducted in an indoor scenario, including multiple locations for the transmitter module. From the capacity analysis, it may be concluded that in indoor environment for corridor scenario, dipoles present better performances than monopoles. However, in NLoS office scenario, monopoles outperforms the dual-polarized antennas. Finally, higher capacity is obtained with higher spacing between radiating elements, due to less correlation among the MIMO subchannels.

On the other hand, a new 2x2 MIMO testbed has been designed and implemented for the future digital television system DVB-T2. The testbed is based on software radio platforms where the signal processing is implemented according to the standard. The testbed has been designed to carry out measurements at the frequency of 594 MHz. A measurements campaign has been done in outdoor and indoor scenarios. Results show the importance of using multiple antennas at each side of the radio link for increasing the capacity of the MIMO system. Moreover, it has also been shown that polarization diversity provides an

additional capacity gain especially for outdoor LoS cases (up to 4 bps/Hz in outage capacity).

6. References

Adjoudani, A.; Beck, E.; Burg, A.; Djuknic, G. M.; Gvoth, T.; Haessig, D.; Manji, S.; Milbrodt, M.; Rupp, M.; Samardzija, D.; Siegel, A.; Sizer II, T.; Tran, C.; Walker, S.; Wilkus, S.A.; Wolniansky, P., "Prototype Experience for MIMO BLAST over Thrid Generation Wireless System," Special Ussue JSAC on MIMO Systems, vol 21, pp. 440-451, April 2003.

Alamouti, S., "A simple transmit diversity technique for wireless communications," IEEE Journal on Selected Areas in Communications, vol. 16, pp. 1451–1458, October 1998.

Aschbacher, E.; Caban, S.; Mehlfuhrer, C.; Maier, G.; Rupp, M., "Design of a flexible and scalable 4x4 MIMO testbed," IEEE 11th Digital Signal Processing Workshop, 2004 and the 3rd IEEE Signal Processing Education Workshop. 1-4 Aug. 2004, pp. 178-181.

Batariere, M. D.; Kepler, J. F.; Krauss, T. P.; Mukthavaram, S.; Porter, L. W.; Vook, F. W., "An experimental OFDM system for broadband mobile communications," IEEE Vehicular Technology Conference, v 4, n 54ND, 2001, p 1947-1951.

Chen, S.-H.; He, W.-H. ; Chen, H.-S. & Lee, Y., "Mode detection, synchronization, and channel estimation for DVB-T OFDM receiver," in IEEE Global Telecommunications Conference, 2003. GLOBECOM '03, vol. 5, Dec. 2003, pp. 2416–2420 vol.5.

Dvb http://www.dvb.org.

Ellingson S. W., "A flexible 4x16 MIMO testbed with 250 MHz – 6 GHz tuning range," IEEE Antennas and Propagation Symposium, Washington, DC, July 2005.

ETSI, "Digital Video Broadcasting (DVB);Frame structure channel coding and modulation for a second generation digital terrestrial television broadcasting system (DVB-T2)," Draft ETSI EN 302 755 V1.1.1 (2008-04), 2008.

Fang, R.-D. & Ma, H.-P., "A DVB-T/H Baseband Receiver for Mobile Environments," in 2007 WSEAS International Conference on Circuits, Systems, Signal and Telecommunications, Queensland, Australia, January 2007.

Foschini, G. & Gans, M., "On Limits of Wireless Communications in a Fading Enviroment when Using Multiple Antennas," Wireless Personal Communications, vol. 6, pp. 311–335, March 1998.

GmbH, "RUSK MIMO: Broadband Vector Channel Sounder for MIMO Channels," MEDAV 2001. Available at http://channelsounder.de/

Goldsmith, A.; Jafar, S.; Jindal, N & Vishwanath, S., "Capacity limits of MIMO channels," IEEE Journal on selected areas in communications, vol. 21, no. 5, June 2003.

Gómez-Calero, C.; García-García, L.; Martínez, R. & de Haro, L., "Comparison of antenna configurations in different scenarios using a wideband MIMO testbed," IEEE Antennas and Propagation Society International Symposium 2006, pp. 301–304, July 2006.

Gómez-Calero, C.; González, L. & Martínez, "Tri-Band Compact Antenna Array for MIMO User Mobile Terminals at GSM 1800 and WLAN bands," Microwave and Optical Technology Letters, vol. 50, no. 7, pp. 1914–1918, July 2008.

Kaiser, T; Wilzeck, A.; Tempel, R., "A modular multi-user MIMO test-bed," IEEE Radio & Wireless Conference 2004, Atlanta Georgia, USA, September, 2004.

Kaiser, T; Wilzeck, A.; Berentsen, M.; Rupp, M., "Prototyping for MIMO Systems – an Overview," Proc. Of the XII European Signal Processing Conference, Vienna (Austria), Oct 2004, pp. 681-688.

Lee, Y.-S.; Kim, H.-N. & Son, K. S., "Noise-Robust Channel Estimation for DVB-T Fixed Receptions," IEEE Transactions on Consumer Electronics, vol. 53, no. 1, pp. 27–32, February 2007.

Mora-Cuevas, J.; Gómez-Calero, C.; Cuéllar, L. & de Haro, L., "A Wideband OFDM MIMO Measurement System for Antenna Evaluation," Antennas and Propagation International Symposium, 2008 IEEE, 5-12 July 2008.

Nallatech http://www.nallatech.com.

Palin, A. & Rinne, J., "Symbol synchronization in OFDM system for time selective channel conditions," in Proceedings of The 6th IEEE International Conference on Electronics, Circuits and Systems, vol. 3, 1999, pp. 1581–1584 vol.3.

Paulraj, A.; Gore, D.; Nabar, R & Bölcskei, H., "An overview of MIMO communications - A key to gigabit wireless," Proceedings of the IEEE, vol. 92, no. 2, pp. 198 – 217, 2004.

Pietsch, C.; Teich W. G.; Lindner, J.; Waldschmidt, C.; Wiesbeck, W., "A highly flexible MIMO demonstrator," International ITG/IEEE Workshop on Smart Antennas WSA 2005. Duisburg, Germany. April 2005.

Sampath, H.; Talwar, S.; Tellado, J.; Erceg, V. & Paulraj A., "A fourthgeneration MIMO-OFDM broadband wireless system: design, performance, and field trial results," IEEE Communications Magazine, vol. 40, no. 9, pp. 143–149, September 2002.

Samuelsson, D.; Jaldén, J.; Zetterberg, P.; Ottersen B., "Realization of a Spatially Multiplexed MIMO System," EURASIP Journal on Applied Signal Processing, March 2005.

Seeger R.; Brotje L.; Kammeyer K. D., "A MIMO hardware demonstrator: application of space-time block codes," Proc. of 3rd IEEE International Symposium on Signal Processing and Information Technology, 2003. ISSPIT 2003. Proceedings, 14-17 Dec. 2003, pp. 98-101.

Signalion www.signalion.com

Stege, M.; Schafer, F.; Henker, M.; Fettweis, G., "Hardware in a loop-a system prototyping platform for MIMO-approaches," ITG Workshop on Smart Antennas, 2004, pp. 216-222.

Telatar, E., "Capacity of multi-antenna Gaussian channels," Eur. Trans. Telecomm. ETT, vol. 10, no. 6, pp. 585–596, November 1999.

van de Beek, J; Sandell, M. & Borjesson, P., "ML estimation of time and frequency offset in OFDM systems," IEEE Transactions on Signal Processing, vol. 45, no. 7, pp. 1800–1805, Jul 1997.

van Zelst, A.; Schenk, T. C. W., "Implementation of a MIMO OFDM-based wireless LAN system," IEEE Transactions on Signal Processing, vol. 52, Issue 2, Feb. 2004, pp. 483-494.